8.334 Statistical Mechanics II
Rich Phase Diagrams of Frustrated Honeycomb Spin Lattices

Yingzhe Tommy Tai

Frustrated magnetism occurs when spins on a lattice are unable to find an orientation to fully satisfy all competing interactions with their neighbours, leading to multiple phases with complex magnetic structure. The Kitaev quantum spin liquid (QSL), one such phase that is highly sought after, curiously exhibits no long-range order even at the lowest temperatures. This is due to the frustrated bond-directional Kitaev interactions on a honeycomb lattice. Yet, no conclusive evidence of a true QSL has been confirmed thus far, with prominent candidate material systems persistently exhibiting long-range order at low enough temperatures. One possible model to account for this observation is the Kitaev-Heisenberg model on the honeycomb lattice. In the classical model, the competition between the anisotropic Kitaev and isotropic Heisenberg interactions leads to a discrete six-state clock model with four collinear magnetic orders at low temperatures. Before the system transitions to a paramagnet at high temperatures, it undergoes a critical Berezinskii-Kosterlitz-Thouless (BKT) phase transition and exhibits correlations with algebraic decay in space.

I. INTRODUCTION

Frustrated magnetism occurs when spins have competing interactions that prevent them from finding an orientation that satisfies all neighbors, leading to rich magnetic phases. One notable example is the Kitaev quantum spin liquid (QSL) [1]. The spins do not magnetically order even at absolute zero temperature, forming a quantum superposition of various spin configurations, giving rise to a highly entangled exotic state of matter, with rich applications in quantum computing [2]. The realization of this QSL ground state requires the spins to be frustrated by nearest neighbour bond-directional 'Ising' interaction on a honeycomb lattice, termed as the Kitaev interaction [3]. Such anisotropic bond-dependent interactions manifest in honeycomb lattice featuring MO_6 (M = Ir or Ru) octahedra that are edge-sharing with 90°M-O-M bonds [4]. The most prominent candidate material system is the honeycomb iridates (A_2IrO_3) where the anisotropic part of the interactions among the Ir-ions has the same form as the Kitaev coupling. Motivated by the rich physics the Kitaev model promises, a large body of experimental work has been devoted to realize this elusive phase of matter. Yet, although these honeycomb lattices are strongly frustrated, they are antiferromagnetically ordered with the transition temperature ranging from 7 to 18 K, and remain ordered till the lowest experimentally accessible temperature [5, 6]. There has thus far been no clear-cut material realization of a quantum spin liquid (QSL).

The persistent presence of long-range order (LRO) at low enough temperatures in materials like Na_2IrO_3 and Li_2IrO_3 indicates either quantum fluctuations, that are essential to destroy LRO, are not dominating in these materials or that the Kitaev QSL phase is fragile against various types of perturbations. From a material perspective, the various stacking disorder and distortions are often characterized by unequal M-M bonds inherent in these honeycomb lattices, posing a daunting experimental challenge in synthesizing them [7]. There is strong evidence that the spin Hamiltonian of these systems are well described by the Kitaev-Heisenberg model [8], where the Heisenberg interaction competes with the Kitaev interaction. A systematic understanding of the resulting phase diagram, even in the classical limit, is thus crucial to account for the observed LRO.

I will introduce the classical Kitaev-Heisenberg model on the honeycomb lattice [9, 10] and explore the rich phase diagram therein. At low temperatures, the competition between the anisotropic Kitaev and isotropic Heisenberg interactions leads to a six-state clock model. Depending on the relative interaction strengths, the ground state is one of the four collinear magnetic orders - the Néel anti-ferromagnet (AFM), a zigzag AFM (the dual of the Néel), the ferromagnet (FM), and the stripy AFM. Before the system transitions to a paramagnet at high temperatures, the system undergoes a critical Berezinskii-Kosterlitz-Thouless (BKT) phase transition and exhibits correlations with continuously variable critical exponents. Characteristic vortex-like topological excitations are also evident here. I will discuss the formulation of this model, the numerical results of the phase transitions reported in Refs. [9, 10], as well as, the ground state magnetic textures that I have simulated with my preliminary Python code implementation of the Metropolis algorithm for this model. Finally, I will comment on various works to account for the observed LRO by introducing additional interactions.

II. CLASSICAL KITAEV-HEISENBERG MODEL

The classical Kitaev-Heisenberg (KH) model is

$$H = -J_K \sum_{\langle i,j\rangle_\gamma} S_i^\gamma S_j^\gamma + J_H \sum_{\langle i,j\rangle} S_i S_j \tag{1}$$

where J_K and J_H denote the FM Kitaev anisotropic exchange and the AFM Heisenberg isotropic exchange. The

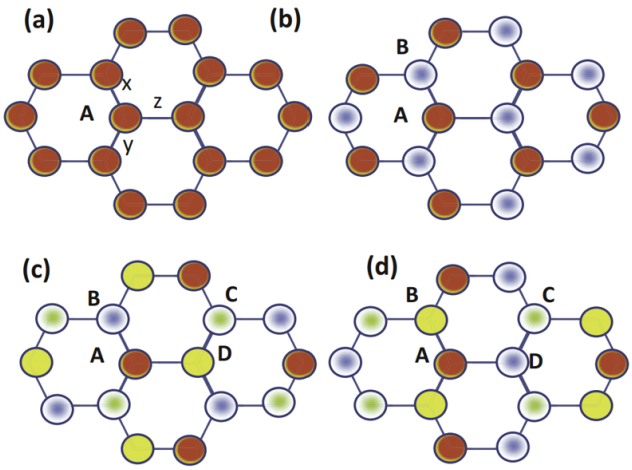

Figure 1. **Four possible magnetic configurations** (a) FM ordering; (b) AFM Néel order; (c) AFM stripy order; (d) AFM zigzag order. Open and filled circles correspond to up and down spins respectively. Reproduced from Ref. [10].

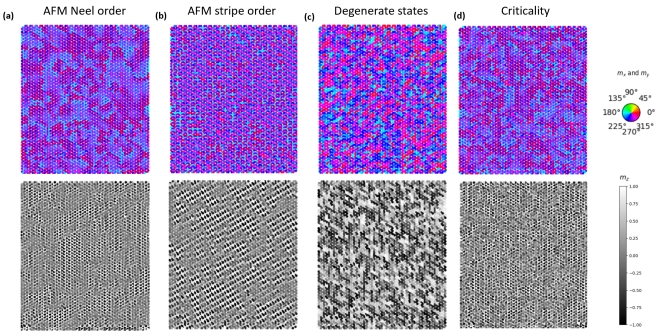

Figure 2. **Simulated ground state configurations for various α regimes** (a) AFM Néel order, (b) AFM stripy order; (c) classically degenerate magnetic orders; (d) Lattice of small vortex-like topological excitations in the critical phase ($\alpha = 0.08$, $T = 0.17$ for 50 by 50 hexagonal unit cells).

AFM Heisenberg exchange is consistent with the AFM order observed in the honeycomb iridates at low temperatures; while the Kitaev exchange is FM and is along the cubic axes of the IrO_6 octahedra, i.e. the three bonds of the honeycomb lattice. As shown later, the presence of Kitaev interactions reduces the symmetry of the system from a continuous SU(2) symmetry to a discrete $\mathbb{Z}_6$ symmetry, thereby permitting the long-range order (LRO) observed in this quasi-two-dimensional system. Otherwise, by the Mermin-Wagner theorem, two-dimensional magnetic systems with just Heisenberg exchange exhibit continuous symmetry and cannot exhibit LRO at any finite temperature. Interestingly, the KH model exhibits a duality transformation via $K \leftrightarrow K+2J$ and $J \leftrightarrow -J$ [11].

A. Low temperature phase

To describe the competition between Kitaev and Heisenberg exchange, their relative strengths are parametrized via $J_K = 2\alpha$ and $J_H = 1 - \alpha$ and describe the magnetically ordered states and their associated order parameter

- $0 < \alpha < 1/3$: AFM Néel order

$$\vec{N} \propto \sum_i (\vec{S}_{i,A} - \vec{S}_{i,B}) \tag{2}$$

  where A and B refer to the standard two sublattices of the honeycomb lattice;

- $1/3 < \alpha < 1$: stripy AFM order

$$\vec{S} \propto \sum_i (\vec{S}_{i,A} - \vec{S}_{i,B} - \vec{S}_{i,C} + \vec{S}_{i,D}) \tag{3}$$

  where the arrangement of A, B, C, and D are illustrated in Fig. 1. The stripy phase is the exact ground state at $\alpha = 0.5$ and can be regarded as a fully polarized 'FM state' in a rotated basis - with spin A fixed and spins B, C, and D rotated by angle π about the x, y, and z axes respectively;

- $\alpha = 1$: the stripy AFM order is classically degenerate with FM order and zigzag AFM order where the latter two are characterized by the order parameters

$$\vec{M} \propto \sum_i \vec{S}_i \tag{4}$$

$$\vec{Z} \propto \sum_i (\vec{S}_{i,A} + \vec{S}_{i,B} - \vec{S}_{i,C} - \vec{S}_{i,D}) \tag{5}$$

  Here, the KH model is frustrated and exhibits a macroscopic degeneracy such that thermal fluctuations of spins are ineffective to remove this degeneracy. Hence, the classical Kitaev model shows no order by disorder. at finite temperatures.

$\alpha = 0$ and $\alpha = 0.5$ are two special points, corresponding to a purely AFM state and the aforementioned 'polarized FM state', where the KH model preserves the continuous SU(2) symmetry. Away from these two points, the Néel and stripy states have an associated quasi-Goldstone mode at the ordering vector (Eqn. 2 and 3 respectively), evidencing the spontaneous breaking of the continuous symmetry [12]. Projecting the vector order parameter ($\vec{N}$ and $\vec{S}$) on the (111) plane reveals a discrete six-fold symmetry, i.e. a $\mathbb{Z}_6$ order parameter. The (111) plane preserves the cubic symmetry of the model and its degeneracy is related to the orientation of the order parameter with respect to the directions in a cubic crystal.

I simulated the ground state for this O(3) model under the various regimes using the standard Metropolis algorithm [13]. This consists of guided random walks through

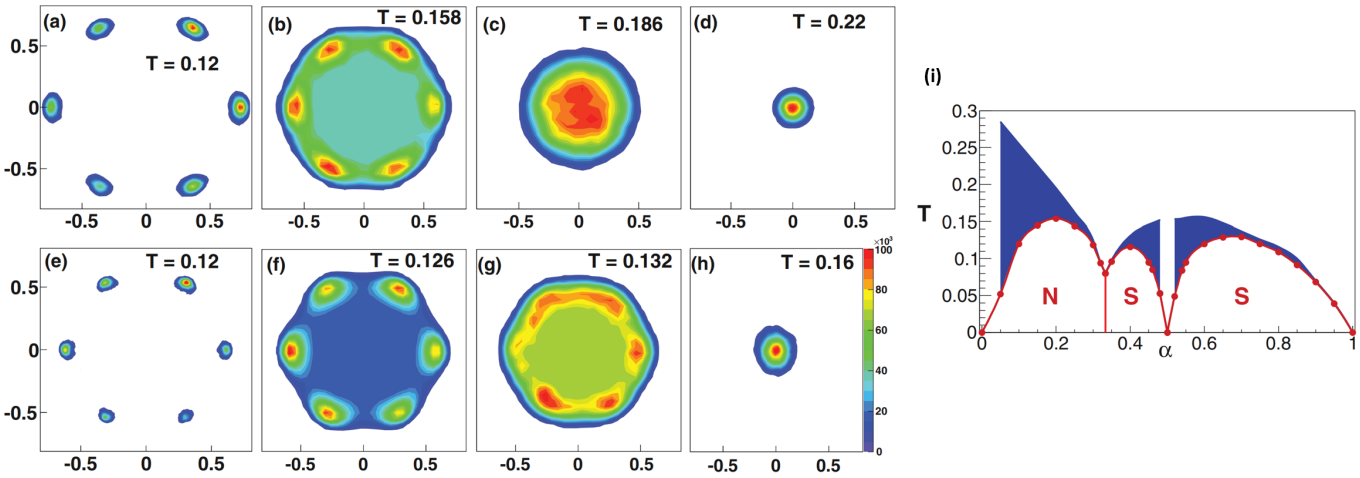

Figure 3. **System transitions from a discrete six-fold symmetry at low temperatures, through a BKT transition, and ends at a disordered paramagnetic phase at high temperatures** (a-h) Histograms of the order parameter $m_{N(S)}$ (Eqn. 6) in the ordered phase (a), (e), in the intermediate phase (b-c), (f-g), and in the disordered phase (d), (h). (a-d) are computed for $\alpha = 0.25$ (Néel) wheras (e-h) are for $\alpha = 0.75$ (stripy). (i) Finite temperature phase diagram with the BKT critical phase bounded in the blue regions. Reproduced from Ref. [10].

phase space and will visit all sites in phase space regardless of initial conditions in the limit of an infinite Monte Carlo steps, i.e. ergodic. To speed up computations, I partitioned the bipartitie honeycomb lattice into two groups (the spins in this model are only coupled to its nearest neighbours and thus members within each group are disconnected) and update all the unconnected spins simultaneously [14] (this still preserves detailed balance). For the O(3) model, we cannot sample the spherical angles uniformly, otherwise the spins will tend to point to the poles [15]. Despite the considerable effort to optimize my code, I am not able to replicate the numerical results in Ref. [10] within a reasonable timeline. Fig. 2 illustrates the simulated ground states, together with the lattice of vortex-like topological excitations in the critical regime, which I will elaborate in the next section.

B. Criticality

The KH model exhibits an interesting critical phase at intermediate temperature that corresponds to a Berezinskii-Kosterlitz-Thouless (BKT) phase transition [16]. This was determined numerically and reported in Ref. [9, 10]. To visually see this phase transition, let's define

$$m_{N(S)} = \sum_{i=1}^{6} |m_{i,N(S)}| e^{i\theta_i} \tag{6}$$

where θ_i is chosen such that the minimal-energy states of the order parameter points along the cubic axes, labelled by $\theta_i = \pi n_i/3$, with $n_i = 0, 1, 2, 3, 4, 5$. Illustrated in Fig. 3(a-h), as the temperature is increased, a transition from an ordered phase (six isolated spots corresponding to a $\mathbb{Z}_6$ symmetry order parameter) through an intermediate critical phase (ring distribution) to the disordered phase (uniform distribution around zero). This critical phase has an emergent, continuous U(1) symmetry. The exact temperature for the BKT transition depends on α and the full phase diagram, that was determined numerically, is illustrated in Fig. 3i.

Both inside the critical phase and at the boundaries, the order parameter exhibits a power-law dependence on system size of the form $m_{N(S)} \sim L^{-\eta/2}$. Renormalization group (RG) analysis of the intermediate phase of the six-state clock model predicts a critical exponent of 1/9 and 1/4 respectively [17]. This was verified numerically using a finite-size-scaling analysis over rather large systems (by sweeping different L, up to $L = 200$) by Ref. [10] for two different α values. The numerical results demonstrate a linear behaviour over a temperature interval with boundaries marked by the lower T_{c_1} and upper temperature T_{c_2} transitions (Fig. 4a,b). The numerical results, as summarized:

α	T_{c_1}	T_{c_2}	η_1	η_2
0.25	0.152	0.162	0.13	0.21
0.75	0.125	0.127	0.13	0.22

are in fairly good agreement with RG. Ref. [10] further verify the estimates for T_{c_1} using Binder cumulants, defined as

$$B_{O=N,S} = 1 - \frac{\langle O \rangle^4}{3\langle O^2 \rangle^2} \tag{7}$$

Using the finite-size-scaling analysis again, the crossing points of the cumulants (Fig. 4c,d) will correspond to the

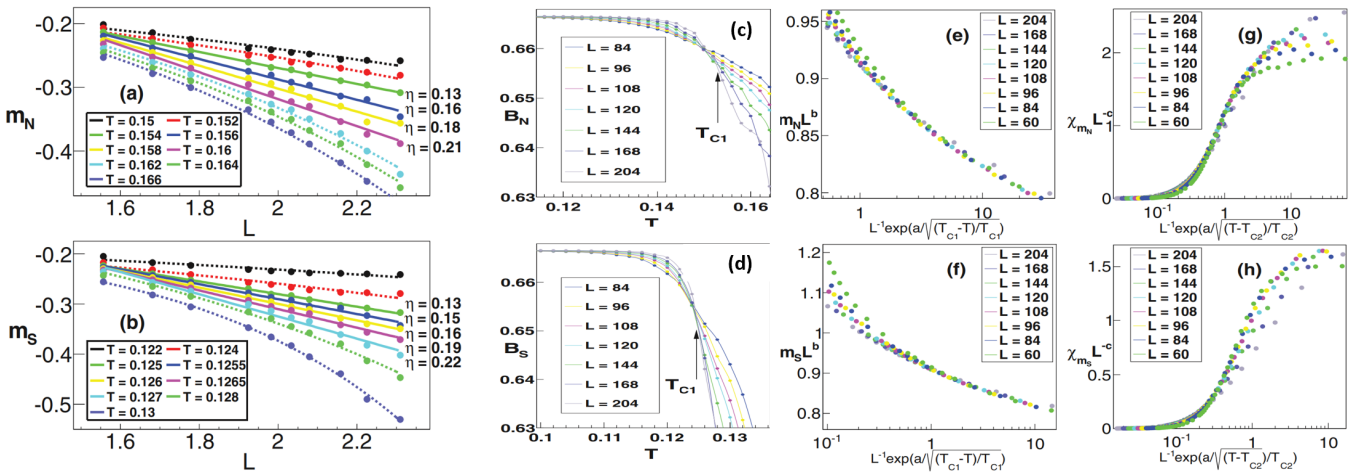

Figure 4. **Finite-size scaling analysis of various thermodynamic quantities** The top row is for the regime $\alpha = 0.25$ (Néel), while the bottom row is for $\alpha = 0.75$ (stripy). (a-b) Log-log plots of the magnetic order parameter to extract the critical exponent η, (c-d) Binder cumulants to extract the lower boundary of the critical phase T_{c_1}, (e-f) power law scaling of magnetic order parameter, and (g-h) susceptibility to extract η's and T_c's for the upper and lower boundary of the critical phase. Reproduced from Ref. [10].

temperature at which the LRO is destroyed [18]. Another way to estimate the critical phase boundaries is to use the finite-size-scaling analysis. This assumes that the singular part of the free energy is a homogeneous function of system size L and of correlation length ξ and depends only on their ratio L/ξ. Based on this assumption, the finite-size-scaling behaviors of the order parameter and the susceptibility have the following functional forms:

$$m_{N(S)} = L^{-b} f_m(L/\xi) \tag{8}$$

$$\chi_{m_{N(S)}} = L^{c} f_\chi(L/\xi) \tag{9}$$

where the scaling parameters are related via $b = \eta/2$ and $c = 2-\eta$. We expect the correlation length near the critical temperature T_c diverges as $\xi \sim e^{at^{1/2}}$, where a is a nonuniversal constant and $t = |T - T_c|/T_c$ is the reduced temperature. Fig. 4e-h show that for different system sizes plotted in their scaled form, the data collapse reasonably well onto universal curves that correspond to the universal functions. The fitted parameters are summarized here:

α	T_{c_1}	T_{c_2}	η_1	η_2
0.25	0.153	0.1615	0.11	0.275
0.75	0.125	0.127	0.11	0.225

III. OTHER EXTENSIONS TO THE MODEL

The first way to extend the model is to allow very generically the Kitaev and the Heisenberg interactions to change sign, which allows the zigzag and FM order as non-degenerate ground states (Eqns. 4-5), which were previously absent. Another extension is to fully break the rotational symmetry by including cubic anisotropy. Another source of frustration that has not been considered in Ref. [10] is the off-diagonal exchange between nearest neighbours [19], that is known to drive Mott insulators into a classical spin liquid regime. While anti-symmetric exchange Dzyaloshinskii-Moriya interactions can be considered [20], they are typically absent since most of Kitaev materials preserve inversion symmetry. A comprehensive recent review of the Kitaev model, beyond the honeycomb iridates is discussed in Ref. [11].

IV. CONCLUSION

In this term project, I studied the classical Kitaev-Heisenberg model, which has been used to account for the observed long-range order in honeycomb iridates despite the evidence of strong Kitaev interactions present in these materials. I simulated the low-temperature ground state and the finite-temperature critical state with the Checkerboard-Metropolis algorithm on the honeycomb lattice. The critical BKT phase transition was studied numerically in Ref. [9, 10] with a high-performance implementation of the Metropolis algorithm. They fully mapped out the phase boundary for all relative Kitaev interaction strengths and temperature, using the Binder cumulants, finite-size scaling of the magnetic order parameter and the susceptibility. The numerical results of the critical exponent agree well with the renormalization group estimate of the six-state clock model.

[1] L. Balents, "Spin liquids in frustrated magnets," *nature*, vol. 464, no. 7286, pp. 199–208, 2010.

[2] C. Nayak, S. H. Simon, A. Stern, M. Freedman, and S. Das Sarma, "Non-abelian anyons and topological quantum computation," *Reviews of Modern Physics*, vol. 80, no. 3, pp. 1083–1159, 2008.

[3] A. Kitaev, "Anyons in an exactly solved model and beyond," *Annals of Physics*, vol. 321, no. 1, pp. 2–111, 2006.

[4] J. Chaloupka, G. Jackeli, and G. Khaliullin, "Mott insulators in the strong spin-orbit coupling limit: From heisenberg to a quantum compass and kitaev models," *Phys. Rev. Lett*, vol. 105, p. 027204, 2010.

[5] X. Liu, T. Berlijn, W.-G. Yin, W. Ku, A. Tsvelik, Y.-J. Kim, H. Gretarsson, Y. Singh, P. Gegenwart, and J. Hill, "Long-range magnetic ordering in na 2 iro 3," *Physical Review B*, vol. 83, no. 22, p. 220403, 2011.

[6] H. Takagi, T. Takayama, G. Jackeli, G. Khaliullin, and S. E. Nagler, "Concept and realization of kitaev quantum spin liquids," *Nature Reviews Physics*, vol. 1, no. 4, pp. 264–280, 2019.

[7] H. Zhao, B. Hu, F. Ye, M. Lee, P. Schlottmann, and G. Cao, "Ground state in proximity to a possible kitaev spin liquid: The undistorted honeycomb iridate na x iro 3 (0.60â‰¤ xâ‰¤ 0.80)," *Physical Review B*, vol. 104, no. 4, p. L041108, 2021.

[8] Y. Singh, S. Manni, J. Reuther, T. Berlijn, R. Thomale, W. Ku, S. Trebst, and P. Gegenwart, "Relevance of the heisenberg-kitaev model for the honeycomb lattice iridates a 2 iro 3," *Physical review letters*, vol. 108, no. 12, p. 127203, 2012.

[9] C. C. Price and N. B. Perkins, "Critical properties of the kitaev-heisenberg model," *Physical review letters*, vol. 109, no. 18, p. 187201, 2012.

[10] C. Price and N. B. Perkins, "Finite-temperature phase diagram of the classical kitaev-heisenberg model," *Physical Review B*, vol. 88, no. 2, p. 024410, 2013.

[11] I. Rousochatzakis, N. Perkins, Q. Luo, and H.-Y. Kee, "Beyond kitaev physics in strong spin-orbit coupled magnets," *Reports on Progress in Physics*, 2024.

[12] J. Chaloupka and G. Khaliullin, "Hidden symmetries of the extended kitaev-heisenberg model: Implications for the honeycomb-lattice iridates a 2 iro 3," *Physical Review B*, vol. 92, no. 2, p. 024413, 2015.

[13] N. Metropolis and S. Ulam, "The monte carlo method," *Journal of the American statistical association*, vol. 44, no. 247, pp. 335–341, 1949.

[14] J. Romero, M. Bisson, M. Fatica, and M. Bernaschi, "High performance implementations of the 2d ising model on gpus," *Computer Physics Communications*, vol. 256, p. 107473, 2020.

[15] M. LeBlanc, *Monte Carlo simulations of inter- and intra-grain spin structure of Ising and Heisenberg models*. PhD thesis, Memorial University of Newfoundland, 2010.

[16] J. M. Kosterlitz and D. J. Thouless, "Ordering, metastability and phase transitions in two-dimensional systems," in *Basic Notions Of Condensed Matter Physics*, pp. 493–515, CRC Press, 2018.

[17] J. Jos, L. Kadanoff, S. Kirkpatrick, and D. Nelson, "Renormalization, vortices, and symmetrybreaking perturbations in the two-dimensional planar model," *Phys. Rev. B*, vol. 16, p. 1217, 1977.

[18] M. Hasenbusch, "The binder cumulant at the kosterlitz–thouless transition," *Journal of Statistical Mechanics: Theory and Experiment*, vol. 2008, no. 08, p. P08003, 2008.

[19] R. Yadav, S. Nishimoto, M. Richter, J. van den Brink, and R. Ray, "Large off-diagonal exchange couplings and spin liquid states in c 3-symmetric iridates," *Physical Review B*, vol. 100, no. 14, p. 144422, 2019.

[20] A. Ralko and J. Merino, "Novel chiral quantum spin liquids in kitaev magnets," *Physical Review Letters*, vol. 124, no. 21, p. 217203, 2020.